Correlation Between Spectral-Domain OCT Findings and Visual Acuity in X-Linked Retinoschisis

Hyun Seung Yang,[1] Jung Bok Lee,[2] Young Hee Yoon,[3] and Joo Yong Lee[3]

[1]Department of Ophthalmology, University of Ulsan, College of Medicine, Ulsan University Hospital, Ulsan, Korea
[2]Department of Statistics, University of Ulsan, College of Medicine, Asan Medical Center, Seoul, Korea
[3]Department of Ophthalmology, University of Ulsan, College of Medicine, Asan Medical Center, Seoul, Korea

Correspondence: Joo Yong Lee, Department of Ophthalmology, University of Ulsan, College of Medicine, Asan Medical Center, 88, Olympic-ro 43-Gil, Songpa-gu, Seoul, Korea 138-736;
ophthalmo@amc.seoul.kr.

Submitted: January 15, 2014
Accepted: March 17, 2014

Citation: Yang HS, Lee JB, Yoon YH, Lee JY. Correlation between spectral-domain OCT findings and visual acuity in X-linked retinoschisis. *Invest Ophthalmol Vis Sci*. 2014;55:3029–3036. DOI:10.1167/iovs.14-13955

Purpose. To investigate the tomographic characteristics of the outer retina and choroid and their relationship with visual acuity in X-linked juvenile retinoschisis (XLRS) patients using spectral-domain optical coherence tomography (SD-OCT).

Methods. In this retrospective, observational, case–control study, we analyzed 20 eyes of 10 patients with XLRS using SD-OCT. The clinical and tomographic features of the outer retina, including the external limiting membrane (ELM), inner segment/outer segment (IS/OS) junction, cone cell outer segment tips (COST) line, photoreceptor outer segment (PROS) length, and choroid, were evaluated. As controls, 40 age-, sex-, and refraction-matched healthy eyes (1:2 matched) were randomly selected and imaged in parallel.

Results. The most prevalent area of abnormality in the outer retina layer of our patients was the outer plexiform layer (OPL; 60% of all affected eyes) and COST line (75% of all affected eyes). On average, the subfoveal choroid and PROS lengths were 35 μm thicker and 19 μm thinner, respectively, in XLRS patients ($P = 0.084$ and $P < 0.001$, respectively). A dominant IS/OS junction, COST line defects, and PROS length were related to patient best-corrected visual acuity (BCVA; $P = 0.029$, $P = 0.001$, and $P < 0.001$, respectively) by univariate analysis. Cone cell outer segment tips line defect and PROS length were the only factors related to BCVA in multivariate analysis ($P = 0.028$ and 0.003, respectively).

Conclusions. Outer plexiform layer and photoreceptor microstructure defects are frequent in XLRS patients. Cone cell outer segment tips line defects and shortened PROS lengths as well as other photoreceptor microstructure defects may be closely related to poor vision in XLRS.

Keywords: X-linked juvenile retinoschisis, foveoschisis, optical coherence tomography, photoreceptors

X-linked juvenile retinoschisis (XLRS) is a rare, early-onset, degenerative disease that affects males with a prevalence of between 1 in 20,000 and 1 in 5000 and causes visual disturbances.[1] The common acquired causes of this visual impairment include macular hole, tractional and rhegmatogenous retinal detachment, vitreous hemorrhage, neovascular glaucoma, and optic atrophy.[2–9] However, poor vision is also often seen in retinoschisis patients lacking the above complications. Although retinal splitting around the fovea may directly cause partial visual loss, the splitting of the inner retinal layer, including the retinal nerve fiber layer (RNFL) and ganglion cell layer (GCL), seen in previous pathology studies[10,11] is not sufficient to explain the progressive visual loss in affected patients. In recent studies, schisis of the inner nuclear layer (INL) and outer nuclear layer (ONL) has also been observed in foveoschisis patients on optical coherence tomography (OCT).[12–14] However, Apushkin and associates[13] reported no correlation between visual acuity, foveal thickness, and cystic area in foveoschisis cases using time-domain OCT.[13] To our knowledge, the photoreceptor and choroidal features and their relationship with visual acuity have never been studied to date, although determining the origin and mechanism of poor vision in patients with XLRS is of the utmost importance.

Our present study aimed to investigate the characteristics of foveal structures, mainly of the outer retina including photoreceptor and choroidal structures, in XLRS patients with spectral-domain OCT (SD-OCT). Correlations between visual acuity and the changes in the retinal and choroidal structures, including the external limiting membrane (ELM), inner segment/outer segment (IS/OS) junction, cone cell outer segment tips (COST) line, photoreceptor outer segment (PROS) length, and choroidal thickness, were also evaluated.

Methods

Study Design

This retrospective, observational, single-center case–control study was performed in accordance with the 1975 Declaration of Helsinki and its 1983 revision and was approved by the institutional review board of the Asan Medical Center, Seoul, South Korea. The computerized clinical charts of consecutive patients diagnosed with treatment-naïve XLRS on SD-OCT, confirmed by detection of a retinoschisis gene (*RS1*) mutation, at the Asan Medical Center between January 1, 2009, and August 31, 2013, were reviewed. Patients were excluded if the quality of the OCT images was insufficient to assess the

integrity or defects of the retinal structures or the choroidal thickness and fixation of eyes was poor. Of the original 25 eyes of 13 patients who met the initial inclusion criteria, five eyes of three patients were excluded for the reasons mentioned above. All of the included eyes (20 eyes of 10 patients) had been examined at least once via spatially encoded SD-OCT (Spectralis; Heidelberg Engineering, Heidelberg, Germany). Each participant underwent a comprehensive ophthalmological examination, including a review of medical and clinical histories; dilated funduscopic examination; slit-lamp biomicroscopy; and measurement of best-corrected visual acuity (BCVA), refraction, and intraocular pressure. Best-corrected visual acuity was measured with a standard Snellen chart and was converted to the logarithm of the minimal angle of resolution (logMAR) for statistical analysis.

To evaluate the discrepancies in the clinical and structural features between the affected eyes and normal eyes, an age-, sex-, and refraction-matched control group with no retinal or choroidal abnormalities was randomly selected. The control group contained 40 eyes of 40 male subjects and was selected using a table of random sampling numbers among 100 eyes of similar age (±1 year) and refraction (±0.5 diopters [D]). The ratio between the number of study eyes and control eyes was 1:2.

OCT Measurements

Optical coherence tomography images were generated using horizontal SD-OCT cross-sectional images (25 lines spaced 240 μm apart) and a central vertical cross-sectional image. All patients were evaluated using the conventional and extended depth image (EDI) modes for Spectralis OCT. For a better image quality, 25 to 30 frames were averaged for each B-scan using spatially encoded SD-OCT. Schisis in the RNFL, GCL, INL, outer plexiform layer (OPL), and ONL was evaluated using vertical and horizontal central OCT images (Figs. A, B). Defects in the outer retinal photoreceptor microstructures, including the ELM, IS/OS junction, and COST line 1 mm from the foveal center, based on the diameter of the physiologic fovea being approximately 2 mm,[15] were also checked using vertical and horizontal central OCT images (Figs. A, B). A COST line defect was defined by an irregularity or definite defect of the line in accordance with previous studies.[16–18] The thickness of the length (Figs. C, D) and choroid were measured manually with the Heidelberg Eye Explorer (version 1.7.1.0; Heidelberg Engineering) in both the study and control eyes by two separate retinal specialists (HSY and JYL). Only central subfield thickness (CST), defined as the average thickness of all points within an inner circle of 1-mm diameter centered on the fovea, was measured automatically after checking and manual adjustment of the reference line. The PROS length was defined as the perpendicular distance from the posterior surface of the IS/OS junction to the anterior surface of the retinal pigment epithelium at foveal center on a horizontal central OCT image.

In the case of subfoveal IS/OS junction discontinuation, the artificial continuous line that connected with the faint posterior border of the IS/OS junction was used as the upper reference line of the PROS lengths. The choroid was measured at five points: subfoveal, 1 mm nasal, 1 mm temporal, 1 mm superior, and 1 mm inferior using vertical and central horizontal EDI OCT sectional images across the fovea. The choroidal thickness was manually calculated as the perpendicular distance from the outer surface of retinal pigment epithelium to the inner surface of the sclera at each point. The presence of specific OCT findings, including retinal schisis and defects, was determined by consensus between two observers (HSY and JYL). The means of the two observer values were used in the PROS thickness and choroidal thickness analysis. An intraclass correlation coefficient (ICC) was used to examine the interobserver agreement in terms of these choroidal thicknesses and PROS length measurement.

Statistical Analysis

All statistical analyses were performed with SAS version 9.1 (SAS Institute, Cary, NC, USA) by a statistical specialist in our institute. Analysis of comparisons between the XLRS and control groups in terms of their clinical and tomographic characteristics was performed by using a linear mixed model for matched samples (1:2 match). Association of clinical and tomographic features was evaluated with Pearson's or Spearman's correlation coefficient. Univariate and multivariate linear regression analysis with backward elimination was used to identify the factors that associated significantly with the tomographic findings and BCVA. A P value < 0.05 was considered to be significant.

Results

Patient Demographic Data

All 20 eyes of the 10 male patients in our study cohort were affected by XLRS bilaterally. The average age of these patients was 17.6 years (range, 6–30 years), and the average refractive error was 0.71 D (range, −4.25 to 7.25). The individual clinical and OCT characteristics of these patients are listed in Table 1. Of the 20 eyes under study, foveoschisis and peripheral retinoschisis were observed in 17 eyes (85%) and 11 eyes (55%), respectively. Three eyes (15%) showed peripheral retinoschisis without foveal extension, and nine eyes (45%) showed only foveoschisis without peripheral extension. Defects in photoreceptor microstructures were detected in 15 eyes (75%), showing an occurrence similar to that of schisis of the inner retinal layer (17 eyes; 85%). Defects in photoreceptor microstructures were present only in eyes with foveoschisis. When the clinical and tomographic data of the patients were compared with those for the control group, BCVA, CST, inferior and nasal choroidal thickness, and PROS lengths showed significant differences between the two groups (Table 2). The average subfoveal choroidal thickness was approximately 35 μm thicker in the patient group, but it failed to achieve statistical significance ($P = 0.084$). Foveoschisis in the INL and OPL and shortened PROS lengths with defects in the ELM, IS/OS junction, and COST line were observed dominantly compared with the matched control eyes (Fig.). Outer plexiform layer schisis was observed frequently (60%) as multiple hyposignal isolated or connected spaces between the hypersignal double-layered OPL in the affected group (Figs. A, B, D). Regarding the manual measurements of choroidal thickness and PROS length, the interobserver agreements were good: The ICCs based on the whole cohort in the subfoveal, nasal, temporal, and superior and inferior choroidal thickness and PROS length measurements were 0.936, 0.905, 0.895, 0.884, 0.891, and 0.916, respectively. The ICCs of each group also revealed good interobserver reliability of the measurements (Table 3).

Tomographic Structural Changes and Their Relationship to Visual Acuity

For our whole study cohort, the mean BCVA (logMAR) was 0.49 ± 0.35. The mean CST, subfoveal choroidal thickness, and PROS length were 425.0 ± 150.3, 358.0 ± 112.5, and 42.0 ± 12.6 μm, respectively. Central subfield thickness, the presence of INL schisis or a dominant IS/OS junction, COST line defects,

Table 1. Clinical and Optical Coherence Tomographic Characteristics of the Study Patients With X-Linked Juvenile Retinoschisis

Eye No.	Age, y	Refractive Error, D	BCVA, logMAR	CST, µm	Subchoroidal Thickness, µm	Foveoschisis				ELM Defect	IS/OS Defect	COST Defect	PROS Length, µm
						GCL	INL	OPL	ONL				
1	6	6.5	0.00	421	311	O	O	O	O	X	X	O	16.0
2	6	6	0.40	429	298.5	O	O	O	X	X	X	O	27.5
3	10	−2.75	0.20	247	188.5	X	X	X	X	X	X	X	42.0
4	10	−4.25	0.70	246	193.5	X	X	X	X	X	X	X	37.0
5	11	2.75	0.90	347	382	X	O	O	X	X	X	X	42.5
6	11	1.5	0.80	276	299	X	O	O	O	X	X	X	46.5
7	12	0.75	0.60	542	229.5	X	O	O	X	O	O	O	23.0
8	12	−1.5	0.49	526	317.5	X	O	O	X	O	O	O	27.0
9	17	6.75	0.52	518	565	X	O	X	X	O	O	O	8.5
10	17	7.25	0.70	837	604.5	X	O	O	O	O	O	O	9.5
11	19	0	0.52	294	345.5	O	O	O	O	X	O	O	21.5
12	19	−3.5	0.40	301	345.5	O	O	X	X	X	X	O	37.0
13	20	−0.25	0.52	463	390	O	O	X	X	X	X	O	35.0
14	20	0	1.30	459	346	O	O	X	X	X	X	O	38.5
15	23	−0.75	0.52	573	478.5	X	O	O	O	O	X	O	35.0
16	23	−3.5	0.70	267	347.5	X	X	X	X	X	X	X	43.0
17	28	−0.5	0.20	259	445.5	X	O	O	X	O	O	O	25.5
18	28	−0.5	0.10	424	467	O	O	O	X	O	O	O	42.0
19	30	0.25	0.10	511	227	O	O	X	X	O	O	O	14.5
20	30	0	0.20	559	377.5	O	O	O	X	O	O	O	11.5
Average	17.6	0.71	0.49	425	358.0	45%, 9 eyes	85%, 17 eyes	60%, 12 eyes	25%, 5 eyes	45%, 9 eyes	45%, 9 eyes	75%, 15 eyes	29.2

O, foveoschisis or defect was found; X, foveoschisis or defect was not found.

Table 2. Study Patient Characteristics and Optical Coherence Tomography Features Including the Central Foveal and Choroidal Thicknesses of X-Linked Juvenile Retinoschisis Compared with Normal Controls

Characteristic	X-Linked Retinoschisis	Control	*P* Value*
Number of eyes	20, 10 patients	40 eyes, 40 patients	1:2 matched
Age, y	17.9 ± 7.8	17.4 ± 7.1	1:2 matched
Sex, men/women	20/0	40/0	1:2 matched
Refractive error, D	0.71 ± 3.48	0.45 ± 3.25	1:2 matched
BCVA, logMAR	0.49 ± 0.35	0.03 ± 0.06	<0.001
CST, μm	425.0 ± 150.3	268.8 ± 16.9	<0.001
Choroidal thickness, subfoveal, μm	358.0 ± 112.5	323.1 ± 75.5	0.084
Choroidal thickness, nasal, μm	332.7 ± 93.8	278.4 ± 75.7	0.002
Choroidal thickness, temporal, μm	327.2 ± 96.6	308.1 ± 58.7	0.214
Choroidal thickness, superior, μm	348.1 ± 116.0	322.0 ± 75.7	0.247
Choroidal thickness, inferior, μm	353.2 ± 97.0	311.7 ± 70.8	0.016
PROS length, μm	29.2 ± 12.4	48.4 ± 6.3	<0.001

* Linear mixed model for matched samples (1:2 match).

and PROS length were found to be significantly related to BCVA in patients with XLRS ($P = 0.031$, 0.014, 0.029, 0.001, and < 0.001) by univariate analysis (Table 4). However, defects of the COST line and the PROS length were the only significant factors related to BCVA in multivariate analysis ($P = 0.028$ and 0.003, respectively). The subfoveal choroidal thickness and presence of ONL schisis were not significantly related to BCVA ($P = 0.263$ and 0.099, respectively). The Spearman correlation coefficients between the factors are shown in Table 5.

The correlations between PROS length and ELM, IS/OS, or COST line defects were very good ($R = -0.567$, –0.663, and –0.692; $P = 0.009$, $P = 0.001$, and $P = 0.001$, respectively), as were those between the IS/OS defect presence and ELM or COST line defects ($R = 0.798$ and 0.522; $P < 0.001$ and $P = 0.018$, respectively). However, no statistically significant correlations were seen between inner retinal schisis and the presence of substantial photoreceptor microstructure defects. In the comparison of foveoschisis layers, the OPL showed a relatively weak but statistically significant correlation with INL schisis and ONL schisis ($R = 0.514$ and 0.471; $P = 0.020$ and 0.036, respectively). The subchoroidal thickness and defect of ELM, IS/OS, and COST showed relatively good correlation with age ($R = 0.480$, 0.507, 0.437, and 0.382, respectively), but the layers of foveoschisis including GCL, INL, OPL, and ONL defects did not show a good correlation with age (Table 5, all $R < 0.3$).

Discussion

X-linked retinoschisis was first thought to be the result of defects or dysfunction in the Müller cells that were related to a negative b-wave evident on electroretinography.[1] However, identification and subsequent analysis of the *RS1* gene and its protein expression have directly implicated altered cell adhesion and cell–cell interaction in the photoreceptors and bipolar cells in XLRS; the protein is believed to help to maintain the cellular organization of the whole retina and structure of the photoreceptor–bipolar synapse but not the Müller cells.[1,19,20] The results of our present study reveal a high prevalence of schisis in the OPL and its correlation with INL and ONL schisis. This highlights an important relationship between OPL defects and the fundamental mechanism of XLRS.

This is also the first study to analyze the tomographic features, including those of the photoreceptor and choroid, of the eyes of XLRS patients with a Spectralis OCT device (Heidelberg Engineering) and to compare some of the OCT features of XLRS eyes with those of normal healthy age-, sex-, and refraction-matched eyes. In a previous pathology-based study, inner retinal abnormalities, including those of the RNFL and GCL, were found to be the main manifestation of this disorder.[10,11] However, a recent in vivo study that used SD-OCT

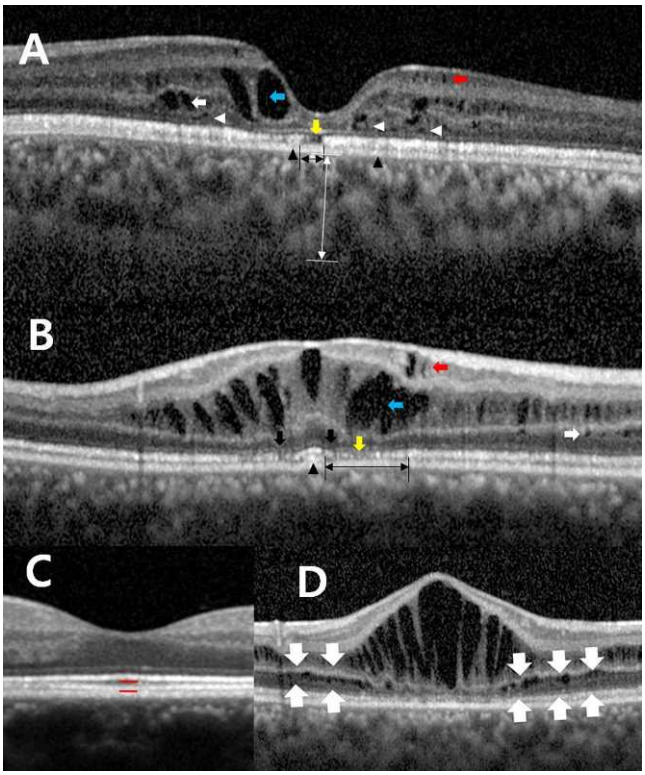

Figure. Spectral-domain optical coherence tomographic images of X-linked juvenile retinoschisis foveoschisis eyes and normal control eyes. Horizontal imagery ([**A**] 11th eye) and vertical imagery ([**B**] 18th eye) revealed defects in the ganglion cell layer (*red arrow*), inner nuclear layer (*blue arrow*), outer plexiform layer (OPL) (*white arrow*), outer nuclear layer (*white arrowhead*), and inner segment/outer segment junction (*yellow arrow*). These images also revealed the cone outer segment tips (COST; *black arrowhead*) line and defects in these structures (range of *black double-headed arrow*). The white *double-headed arrow* depicts the subfoveal choroidal thickness. (**C**) Spectral-domain optical coherence tomography image of a normal control eye showing the photoreceptor outer segment (PROS) length (between the *red lines*). (**D**) Spectral-domain optical coherence tomography image of an XLRS-affected eye (20th eye) showing a shortened PROS length and defect in the OPL (between the *matched white arrows*).

Table 3. Interobserver Reliability and Average Absolute Deviation in the PROS Length and Choroidal Thickness Measurements Between Two Observers

Factors	Group	ICC Analysis			Average Absolute Deviation
		ICC	95% CI	*P* Value	
PROS length, μm	XLRS group	0.917	0.866–0.968	<0.001	2.1
	Control group	0.926	0.901–0.951	<0.001	1.5
Choroidal thickness, subfoveal, μm	XLRS group	0.930	0.875–0.985	<0.001	17.1
	Control group	0.941	0.894–0.988	<0.001	17.0
Choroidal thickness, nasal, μm	XLRS group	0.906	0.847–0.965	<0.001	12.2
	Control group	0.905	0.831–0.979	<0.001	16.7
Choroidal thickness, temporal, μm	XLRS group	0.892	0.822–0.962	<0.001	19.5
	Control group	0.896	0.836–0.956	<0.001	27.1
Choroidal thickness, superior, μm	XLRS group	0.884	0.830–0.938	<0.001	15.0
	Control group	0.883	0.822–0.944	<0.001	14.7
Choroidal thickness, inferior, μm	XLRS group	0.882	0.817–0.947	<0.001	13.0
	Control group	0.899	0.833–0.965	<0.001	17.9

CI, confidence interval.

showed that outer retinal abnormalities were also prevalent.[12–14,21] Our current study findings also support the results of that SD-OCT study, that is, by revealing that the main manifestation of schisis is at the INL (85%) and/or one of the outer retinal layers (85%). However, the most prevalent area of schisis or defect, when confined to the outer retina layer (including photoreceptor layers), was found in the OPL (60%) and COST line (75%).

The COST line is the outer area of the IS/OS junction and reflects the retrograde damage of photoreceptors.[22,23] The COST line of the epiretinal membrane was found to be one of main visual prognostic factors in a previous study.[23] In that study, the vertical force of the retinal surface mechanically affected the outer retina and COST line defect, and it was suggested that the COST line defect may reflect the initial changes of the photoreceptor defect.[23] In our present study, likewise, we speculated that the expansion of the intraretinal cystic lesion could cause stretching of adjacent Müller cells and focal compression of outer retinal microstructures in XLRS eyes. Furthermore, the time-line organization for our XLRS patients, which showed a good correlation between the age and the defect of photoreceptor microstructures, may support the progressive photoreceptor loss over time due to the mechanism. Consequently, the presumed shear forces arising from the intraretinal space may result in damage to photoreceptor microstructures.

The PROS length reflects the thinning of the outer segment of the photoreceptors and defects in the COST line and IS/OS junction.[24–27] In our present study the PROS length was significantly thinner in the XLRS eyes compared with the control eyes (29.3 and 48.4 μm, respectively). The PROS lengths in the control eyes are similar to those reported previously (35–54 μm, depending on the measurement methods used, OCT device, age, and disease).[24–26,28] In addition, the PROS length was also found to be significantly shortened in the affected eyes and showed a very good negative correlation with photoreceptor microstructure defects. In multivariate analysis, COST line defects and the PROS lengths were found to be statistically related to visual acuity. In addition, the presence of an IS/OS junction defect correlated with visual acuity in univariate analysis, though not in multivariate analysis. Thus, a change in the photoreceptor microstructure may be more useful than the detection of intraretinal schisis itself in evaluating the functional condition of XLRS patients.

Advances in imaging with SD-OCT in an EDI mode and swept-source OCT have also greatly increased our ability to visualize the choroid, and thereby enabled a better understanding of the role played by the choroid in different diseases.[29] In our present study, these imaging techniques permitted good visualization of the outer retina and choroid. The ICC of the choroidal structure was excellent in every choroid location, although it was slightly lower than that of previous studies, possibly due to a thick CST and foveoschisis.[30–32] Although no significant difference ($P = 0.084$) was found between the subfoveal choroidal thicknesses of the two

Table 4. Univariate and Multivariate Analyses to Determine the Influence of Tomographic Structural Features on Best-Corrected Visual Acuity in Patients With X-Linked Retinoschisis

Factor	Univariate Analysis		Multivariate Analysis, R^2, 0.707	
	Regression Coefficient B	*P* Value	Standardized Coefficient Beta	*P* Value
CST, μm	0.001	0.031		
Subfoveal choroidal thickness, μm	0.001	0.151	−0.198	0.263
Presence of GCL schisis	0.190	0.187		
Presence of INL schisis	0.463	0.014		
Presence of OPL schisis	0.193	0.185		
Presence of ONL schisis	0.222	0.178	0.225	0.099
Presence of dominant ELM defect	0.240	0.090		
Presence of dominant IS/OS junction defect	0.301	0.029		
Presence of dominant COST defect	0.498	0.001	0.409	0.028
PROS length, μm	−0.020	<0.001	−0.632	0.003

R^2, coefficient of multiple determination.

Table 5. Correlation Coefficients of Clinical and Tomographic Features of the Study Patients With X-Linked Juvenile Retinoschisis

Correlation Coefficient	BCVA, logMAR	Age, y	CST, µm	Subchoroidal Thickness, µm	Foveoschisis				ELM Defect	IS/OS Defect	COST Defect	PROS Length
					GCL	INL	OPL	ONL				
BCVA, logMAR,	1.000	0.123	0.452	0.263	0.281	0.563	0.294	0.232	0.492	0.641	0.736	**−0.855**
P value	–	0.605	0.046	0.263	0.230	0.010	0.208	0.325	0.028	0.002	0.000	**0.000**
Age, y,		1.000	0.275	**0.480**	0.262	0.219	−0.107	−0.181	**0.507**	0.437	0.382	−0.151
P value		–	0.241	**0.032**	0.264	0.353	0.655	0.445	**0.022**	0.054	0.097	0.525
CST, µm,			1.000	0.413	0.096	0.595	0.283	0.130	0.654	0.427	0.651	−0.584
P value			–	0.070	0.688	0.006	0.226	0.584	0.002	0.060	0.002	0.007
Subfoveal choroidal thickness, µm,				1.000	−0.078	0.401	0.204	0.160	0.410	0.262	0.351	−0.193
P value				–	0.742	0.080	0.389	0.500	0.073	0.265	0.130	0.415
Presence of GCL schisis,					1.000	0.380	−0.082	−0.058	−0.212	−0.010	0.522	−0.174
P value					–	0.098	0.731	0.808	0.369	0.966	0.018	0.462
Presence of INL schisis,						1.000	**0.514**	0.243	0.380	0.380	0.728	−0.425
P value						–	**0.020**	0.303	0.098	0.098	0.000	0.061
Presence of OPL schisis,							1.000	**0.471**	0.328	0.328	0.236	−0.177
P value							–	**0.036**	0.158	0.158	0.317	0.455
Presence of ONL schisis,								1.000	−0.058	−0.058	0.067	−0.160
P value								–	0.808	0.808	0.780	0.499
Presence of dominant ELM defect,									1.000	0.798	0.522	**−0.567**
P value									–	0.000	0.018	**0.009**
Presence of dominant IS/OS junction defect,										1.000	0.522	**−0.663**
P value										–	0.018	**0.001**
Presence of dominant COST defect,											1.000	**−0.692**
P value											–	**0.001**
PROS length,												1.000
P value												–

The clinically important correlation coefficients are bolded.

groups in our present study, the choroidal thickness in eyes with XLRS was more likely to be thicker than that of the age and refraction matched normal eyes ($P = 0.002$ and $P = 0.016$, respectively). In addition, the subfoveal choroidal thickness in the eyes with XLRS (358.0 μm) in our current cohort showed a relatively thick choroid compared with that reported in previous studies based on the normal pediatric population. However, the choroidal thickness in our normal eyes (323.1 μm) showed a value similar to that in previous studies; the average subfoveal choroidal thickness in the literature is reported at 312.9 μm based on analyses of 10-year-old patients, 324.2 μm based on children 7 years or older, and 330 μm based on 4- to 12-year-old patients.[33–35] Although not directly shown by our results, a thick choroid may also play a role in XLRS. Thus, the structural characteristics of XLRS do not seem to be limited to the inner retina but extend to the outer retina and include PROS length and the choroid, findings that should be taken into account in future choroidal studies of patients with XLRS.

Our present study has some noteworthy limitations, including its retrospective design; our analyses were not based on longitudinal changes during a long-term follow-up with certain treatments. In addition, the small occurrence rate of XLRS and the difficulty in measuring the horizontal length of the defects in photoreceptor microstructures or quantification of the schisis may lead to the reduced statistical significance of individual tomographic features, as mentioned above. However, our well-matched 1:2 analysis, which used patients who were carefully selected according to strict criteria by retinal specialists (HSY and JYL), enabled us to alleviate these limitations to a certain extent. There was still a possibility of signal interference, which can lead to an overestimation of defects in the outer retinal microstructure caused by severe foveoschisis and a consequent thick retina. Higher-resolution OCT measurements of the length of the outer retinal microstructure defects may permit more precise analysis in the future and also the identification of more significant factors related to BCVA in XLRS patients.

In conclusion, OPL schisis and microstructure defects related to photoreceptors are frequently observed in SD-OCT examinations of patients with XLRS. In addition, abnormalities in the outer retina, including COST line defects and a shortened PROS length, appear to be closely related to poor visual acuity. These clinical and tomographic characteristics should be considered when managing patients to prevent progressive visual deterioration and improve visual prognosis.

Acknowledgments

Disclosure: **H.S. Yang**, None; **J.B. Lee**, None; **Y.H. Yoon**, None; **J.Y. Lee**, None

References

1. Molday RS, Kellner U, Weber BH. X-linked juvenile retinoschisis: clinical diagnosis, genetic analysis, and molecular mechanisms. *Prog Retin Eye Res*. 2012;31:195–212.
2. Zuo C, Chen C, Xing Y, Du L. Neovascular glaucoma in a patient with X-linked juvenile retinoschisis. *Yan Ke Xue Bao*. 2005;21:140–141, 151.
3. Hung JY, Hilton GF. Neovascular glaucoma in a patient with X-linked juvenile retinoschisis. *Ann Ophthalmol*. 1980;12:1054–1055.
4. Lee JJ, Kim JH, Kim SY, Park SS, Yu YS. Infantile vitreous hemorrhage as the initial presentation of X-linked juvenile retinoschisis. *Korean J Ophthalmol*. 2009;23:118–120.
5. Fong DS, Frederick AR Jr, Blumenkranz MS, Walton DS. Exudative retinal detachment in X-linked retinoschisis. *Ophthalmic Surg Lasers*. 1998;29:332–335.
6. Shanmugam MP, Nagpal A. Foveal schisis as a cause of retinal detachment secondary to macular hole in juvenile X-linked retinoschisis. *Retina*. 2005;25:373–375.
7. Sobrin L, Berrocal AM, Murray TG. Retinal detachment 7 years after prophylactic schisis cavity excision in juvenile X-linked retinoschisis. *Ophthalmic Surg Lasers Imaging*. 2003;34:401–402.
8. Laatikainen L, Tarkkanen A, Saksela T. Hereditary X-linked retinoschisis and bilateral congenital retinal detachment. *Retina*. 1987;7:24–27.
9. Turut P, Guthman R, Pfaelzer I, Malthieu D. Vitreous hemorrhage and sex linked juvenile retinoschisis [in French]. *Bull Soc Ophtalmol Fr*. 1984;84:475–477.
10. Manschot WA. Pathology of hereditary juvenile retinoschisis. *Arch Ophthalmol*. 1972;88:131–138.
11. Yanoff M, Kertesz Rahn E, Zimmerman LE. Histopathology of juvenile retinoschisis. *Arch Ophthalmol*. 1968;79:49–53.
12. Yu J, Ni Y, Keane PA, Jiang C, Wang W, Xu G. Foveomacular schisis in juvenile X-linked retinoschisis: an optical coherence tomography study. *Am J Ophthalmol*. 2010;149:973–978, e972.
13. Apushkin MA, Fishman GA, Janowicz MJ. Correlation of optical coherence tomography findings with visual acuity and macular lesions in patients with X-linked retinoschisis. *Ophthalmology*. 2005;112:495–501.
14. Leng T. Two cases of X-linked retinoschisis with different spectral domain optical coherence tomography findings. *Clin Ophthalmol*. 2012;6:1563–1565.
15. Hogan MJ, Alvarado JA, Weddell JE. *Histology of the Human Eye: An Atlas and Textbook*. Philadelphia: Saunders; 1971: 393–522.
16. Ahn SJ, Woo SJ, Kim KE, Jo DH, Ahn J, Park KH. Optical coherence tomography morphologic grading of macular commotio retinae and its association with anatomic and visual outcomes. *Am J Ophthalmol*. 2013;156:994–1001, e1001.
17. Itoh Y, Inoue M, Rii T, Hirota K, Hirakata A. Correlation between foveal cone outer segment tips line and visual recovery after epiretinal membrane surgery. *Invest Ophthalmol Vis Sci*. 2013;54:7302–7308.
18. Itoh Y, Inoue M, Rii T, Hiraoka T, Hirakata A. Correlation between length of foveal cone outer segment tips line defect and visual acuity after macular hole closure. *Ophthalmology*. 2012;119:1438–1446.
19. Molday LL, Wu WW, Molday RS. Retinoschisin (RS1), the protein encoded by the X-linked retinoschisis gene, is anchored to the surface of retinal photoreceptor and bipolar cells through its interactions with a Na/K ATPase-SARM1 complex. *J Biol Chem*. 2007;282:32792–32801.
20. Molday LL, Hicks D, Sauer CG, Weber BH, Molday RS. Expression of X-linked retinoschisis protein RS1 in photoreceptor and bipolar cells. *Invest Ophthalmol Vis Sci*. 2001;42:816–825.
21. Gregori NZ, Berrocal AM, Gregori G, et al. Macular spectral-domain optical coherence tomography in patients with X linked retinoschisis. *Br J Ophthalmol*. 2009;93:373–378.
22. Park SJ, Woo SJ, Park KH, Hwang JM, Chung H. Morphologic photoreceptor abnormality in occult macular dystrophy on spectral-domain optical coherence tomography. *Invest Ophthalmol Vis Sci*. 2010;51:3673–3679.
23. Shimozono M, Oishi A, Hata M, et al. The significance of cone outer segment tips as a prognostic factor in epiretinal membrane surgery. *Am J Ophthalmol*. 2012;153:698–704.
24. Hashimoto Y, Saito W, Saito M, et al. Retinal outer layer thickness increases after vitrectomy for epiretinal membrane, and visual improvement positively correlates with photoreceptor outer segment length. *Graefes Arch Clin Exp Ophthalmol*. 2014;252:219–226.

25. Shiono A, Kogo J, Klose G, et al. Photoreceptor outer segment length: a prognostic factor for idiopathic epiretinal membrane surgery. *Ophthalmology*. 2013;120:788–794.
26. Forooghian F, Stetson PF, Meyer SA, et al. Relationship between photoreceptor outer segment length and visual acuity in diabetic macular edema. *Retina*. 2010;30:63–70.
27. Guerin CJ, Lewis GP, Fisher SK, Anderson DH. Recovery of photoreceptor outer segment length and analysis of membrane assembly rates in regenerating primate photoreceptor outer segments. *Invest Ophthalmol Vis Sci*. 1993;34:175–183.
28. Srinivasan VJ, Monson BK, Wojtkowski M, et al. Characterization of outer retinal morphology with high-speed, ultrahigh-resolution optical coherence tomography. *Invest Ophthalmol Vis Sci*. 2008;49:1571–1579.
29. Mrejen S, Spaide RF. Optical coherence tomography: imaging of the choroid and beyond. *Surv Ophthalmol*. 2013;58:387–429.
30. Branchini L, Regatieri CV, Flores-Moreno I, Baumann B, Fujimoto JG, Duker JS. Reproducibility of choroidal thickness measurements across three spectral domain optical coherence tomography systems. *Ophthalmology*. 2012;119:119–123.
31. Ikuno Y, Maruko I, Yasuno Y, et al. Reproducibility of retinal and choroidal thickness measurements in enhanced depth imaging and high-penetration optical coherence tomography. *Invest Ophthalmol Vis Sci*. 2011;52:5536–5540.
32. Spaide RF, Koizumi H, Pozzoni MC. Enhanced depth imaging spectral-domain optical coherence tomography. *Am J Ophthalmol*. 2008;146:496–500.
33. Ruiz-Moreno JM, Flores-Moreno I, Lugo F, Ruiz-Medrano J, Montero JA, Akiba M. Macular choroidal thickness in normal pediatric population measured by swept-source optical coherence tomography. *Invest Ophthalmol Vis Sci*. 2013;54:353–359.
34. Read SA, Collins MJ, Vincent SJ, Alonso-Caneiro D. Choroidal thickness in childhood. *Invest Ophthalmol Vis Sci*. 2013;54:3586–3593.
35. Park KA, Oh SY. Choroidal thickness in healthy children. *Retina*. 2013;33:1971–1976.

Investigative Ophthalmology & Visual Science